Contrib Mineral Petrol (2005) 149: 600–612
DOI 10.1007/s00410-005-0670-y

ORIGINAL PAPER

Séverine Jannot · Pierre Schiano · Pierre Boivin

Melt inclusions in scoria and associated mantle xenoliths of Puy Beaunit Volcano, Chaîne des Puys, Massif Central, France

Received: 15 October 2004 / Accepted: 25 March 2005 / Published online: 14 May 2005

Abstract In order to characterize the composition of the parental melts of intracontinental alkali-basalts, we have undertaken a study of melt and fluid inclusions in olivine crystals in basaltic scoria and associated upper mantle nodules from Puy Beaunit, a volcano from the Chaîne des Puys volcanic province of the French Massif Central (West-European Rift system). Certain melt inclusions were experimentally homogenised by heating-stage experiments and analysed to obtain major- and trace-element compositions. In basaltic scoria, olivine-hosted melt inclusions occur as primary isolated inclusions formed during growth of the host phase. Some melt inclusions contain both glass and daughter minerals that formed during closed-system crystallisation of the inclusion and consist mainly of clinopyroxene, plagioclase and rhönite crystals. Experimentally rehomogenised and naturally quenched, glassy inclusions have alkali-basalt compositions (with SiO_2 content as low as 42 wt%, $MgO > 6$ wt%, $Na_2O + K_2O > 5$ wt%, Cl∼1,000–3,000 ppm and S∼400–2,000 ppm), which are consistent with those expected for the parental magmas of the Chaîne des Puys magmatic suites. Their trace-element signature is characterized by high concentration(s) of LILE and high LREE/HREE ratios, implying an enriched source likely to have incorporated small amounts of recycled sediments. In olivine porphyroclasts of the spinel peridotite nodules, silicate melt inclusions are secondary in nature and form trails along fracture planes. They are generally associated with secondary CO_2 fluid inclusions containing coexisting vapour and liquid phases in the same trail. This observation and the existence of multiphase inclusions consisting of silicate glass and CO_2-rich fluid suggest the former existence of a CO_2-rich silicate melt phase. Unheated glass inclusions have silicic major-element compositions, with normative nepheline and olivine components, ∼58 wt% SiO_2, ∼9 wt% total alkali oxides, < 3 wt% FeO and MgO. They also have high chlorine levels (> 3,000 ppm) but their sulphur concentrations are low (< 200 ppm). Comparison with experimental isobaric trends for peridotite indicates that they represent high-pressure (∼1.0 GPa) trapped aliquots of near-solidus partial melts of spinel peridotite. Following this hypothesis, their silica-rich compositions would reflect the effect of alkali oxides on the silica activity coefficient of the melt during the melting process. Indeed, the silica activity coefficient decreases with addition of alkalis around 1.0 GPa. For mantle melts coexisting with an olivine-orthopyroxene-bearing mineral assemblage buffering SiO_2 activity, this decrease is therefore compensated by an increase in the SiO_2 content of the melt. Because of their high viscosity and the low permeability of their matrix, these near-solidus peridotite melts show limited ability to segregate and migrate, which can explain the absence of a chemical relationship between the olivine-hosted melt inclusions in the nodules and in basaltic scoria.

Communicated by T.L. Grove

S. Jannot (✉) · P. Schiano · P. Boivin
Laboratoire Magmas et Volcans,
OPGC-Université Blaise Pascal-CNRS,
5 rue Kessler, 63038 Clermont-Ferrand, France
E-mail: s.jannot@opgc.univ-bpclermont.fr
Fax: +33-4-73346744

Introduction

The origin of intracontinental alkali basalts has attracted a great deal of interest among Earth scientists in recent years. This interest has been stimulated by the characteristic features of alkaline lavas, which show a typical enrichment in incompatible elements and have isotopic compositions similar to those of oceanic basalts. In addition, some alkali basalts contain xenoliths of mantle origin, which have trace-element and mineralogical characteristics that provide direct evidence for the existence of metasomatically enriched portions of the upper mantle. Among the petrogenetic problems raised by the study of alkali basalts, the most discussed are

probably the attainment of peralkalinity, the association of contrasting undersaturated and saturated alkaline magma compositions in intracontinental magmatic provinces, the depth of derivation of alkaline magmas and the variation in the source materials from which alkaline magmas are derived. For the latter, emphasis has alternatively shifted from the predominant contribution of the lithosphere as a source of alkali basalts to the asthenospheric mantle, with the recognition of metasomatism and its possible role as a precursor of alkaline magmatism.

A major occurrence of alkaline rocks is provided by the Cenozoic rift system of Central and Western Europe, which includes the French Massif Central. The Tertiary and Quaternary volcanoes of the Massif Central have been extensively studied by the others (e.g. Wilson and Downes 1992; Barruol and Granet 2002). In detail, the nature of their sources is still a matter of debate which centres on the relative importance of the contribution from the metasomatized lithosphere through which the magmas were emplaced and the asthenospheric mantle source of the primary magmas (e.g., Wilson and Downes 1992). There are different and opposite hypotheses for the generation of the volcanism within the Massif Central in the literature. Froidevaux et al. (1974) and Granet et al. (1995) have ascribed the volcanism to the upwelling of a mantle plume. An alternative hypothesis is one that calls on the presence of an asthenospheric flow induced by the formation of the Alpine lithospheric root (Merle and Michon 2001) or the retreat and sinking of the Tethys slab (Barruol and Granet 2002).

Within our present study, we aim to better understand the volcanic system of the Massif Central and what its sources may be by studying the composition of primitive magmas. These magmas are preserved as melt inclusions in olivine crystals in basaltic scoria and associated upper mantle xenoliths from Puy Beaunit, a volcano from the Chaîne des Puys volcanic province of the Massif Central. In the basalts, the melt inclusions contain small quantities of silicate melt that were included in phenocrysts during growth of the crystal structure. Formed at different stages of evolution of the melts, they will thus record the liquid line of descent of magmatic systems (Schiano 2003, and references therein). In mantle derived nodules, the aliquots of natural mantle melts can be preserved as melt inclusions within the minerals that make up the nodule (e.g., Schiano and Clocchiatti 1994).

Here, we examine the composition of the inclusions with the following objectives in mind: (1) to assess the differences in composition between mantle melts preserved in the lithospheric mantle nodules and the primitive melts of the erupted basalts, (2) to evaluate the role of melts preserved in nodules as potential metasomatic agents of the upper mantle, (3) to discuss plausible models for their formation, and (4) to examine their relationship with the magmatic series of the Chaîne des Puys.

Geological setting

The tectonic setting of the magmatic province of western and central Europe is dominated by the Hercynian orogeny, with a major continental collision episode dated at ~360 Ma (Matte, 1986). This event led to the main Hercynian terrane boundaries, which divide the region (Franke 1989). From upper Eocene to early Miocene, a rifting episode has affected the West-European plate and has generated an extensive rift system, which includes the Limagne, Bresse, Rhine, Ruhr, Leine and Eger grabens. This has evolved contemporaneously with the later phases of the alpine orogeny and the Neogene collapse of the Mediterranean and Panomian basins (Ziegler 1982). Associated magmatism occurred from the Paleocene to the Holocene and was restricted to only a few widely scattered districts.

The Massif Central area is the largest magmatic province of the West-European Rift system. It consists of typical intraplate alkaline series (e.g., Villemant et al 1980) that have erupted during two major episodes, from upper Oligocene to early Miocene and from upper Miocene to Pliocene, respectively. The Massif Central consists of many individual volcanic provinces (Fig. 1);

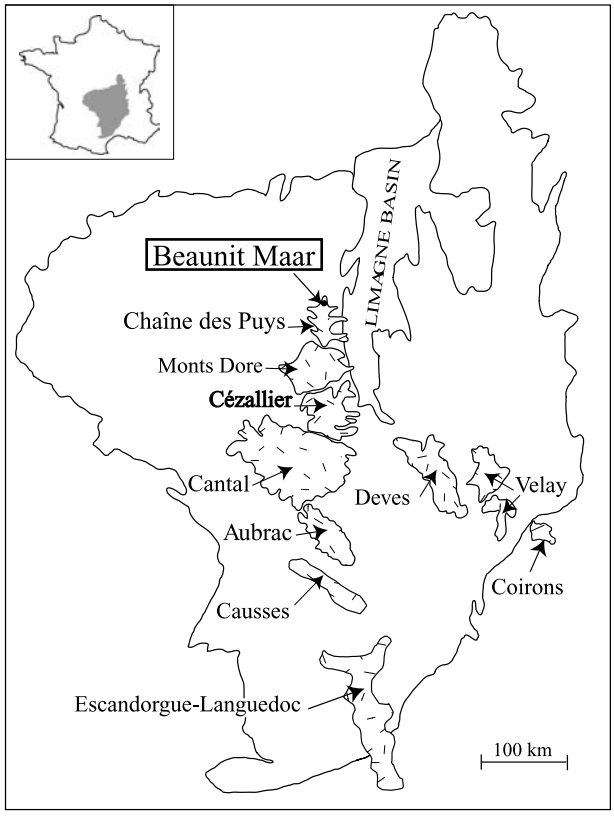

Fig. 1 Distribution of the main volcanic provinces of the French Massif Central: Chaîne des Puys, Monts Dore, Cézallier, Cantal, Aubac, Deves, Velay, Coirons, Causses and Escandorgue-Languedoc. The peridotite nodule and scoria samples mentioned in the text are from Puy Beaunit, a maar located at the northern end of the Chaîne des Puys

the Cantal (20–7 Ma), Causses (14–2 Ma), Velay (11–6 Ma), Aubrac (8–6 Ma), Coiron (8–5.5 Ma), Cézallier (7.8–2.5 Ma), Escandorgue-Languedoc (3.5–0.8 Ma), Deves (3–0.5 Ma), Monts Dore (3–0.25 Ma) and the Chaîne des Puys (95–7 Ka). The Chaîne des Puys consists of a hundred young well-preserved volcanoes that have formed on the top of a horst overhanging the Limagne basin. Volcanic products from the Chaîne des Puys have a K-rich alkaline affinity, ranging in composition from basalt to trachyte.

The basaltic scoria and mantle xenolith samples selected for this study were sampled at the Puy Beaunit volcano vent, which is the largest maar of the Chaîne des Puys. It is dated at 54,000 ± 7,000 years (Miallier et al. in Boivin et al. 2004) and has been formed during a phreatomagmatic event, which has subsequently evolved into a strombolian eruption leading to the formation of a scoria cone (Puy Gonnard). Previous studies (e.g. Faure et al. 2001; Féménias et al. 2001) have shown that the Puy Beaunit extrusives contains a great variety of xenoliths from the upper crust, lower crust and upper mantle.

Experimental and analytical techniques

Mineral separation

In order to separate potential inclusion-bearing crystals, basaltic scoria and mantle xenoliths were gently crushed, followed by a heavy liquid mineral separation. A binocular microscope was used to handpick olivine crystals. Finally, these olivines were mounted in epoxy on microscope slides for grinding and polishing on both sides.

High-temperature microthermometry

High-temperature thermometry experiments on olivine-hosted melt inclusions were performed at ambient pressure with a heating stage at LMV (Laboratoire Magmas et Volcans, Clermont-Ferrand). Experimental study of melt inclusions aims to reverse phase changes that occurred inside the inclusion during natural cooling, such as crystallisation and formation of the shrinkage/fluid bubble, by reheating the inclusion up to the temperature at which it was trapped and then quenching the restored trapped liquid for further analysis. We carefully selected partially crystallised melt inclusions with a well-developed shrinkage bubble and no evidence of heterogeneity. The heating stage is composed of a heating coil and a sample holder located in its centre (Sobolev et al. 1980) and is placed under an optical microscope which allows visual monitoring of individual melt inclusions during the experiment. The temperature is measured with a $Pt_{90}Rh_{10}$ thermocouple that is welded to the sample holder and calibrated with compounds with known melting points. Experiments have been performed in a He atmosphere purified with Zr at 700°C to avoid oxidation of the host mineral. The accuracy of the temperature determination is about ±10°C at the maximum temperature and the thermal gradient along the samples is less than 10°C. Experiments were run at a range of heating rates and exposure times in order to assess the effects caused by variations in the rate of the transformations in the inclusions. The optimal experimental conditions ensuring equilibration during homogenisation of the inclusions correspond to heating rates of around 30°C·min^{-1} from 20°C to 850°C and 3–5°C·min^{-1} for $T > 850$°C. After quenching, the samples were polished to expose the inclusions for electron microprobe analysis.

Electron microprobe analysis

Electron microprobe analyses were carried out at the LMV using a Camebax SX 100 electron microprobe with an accelerating voltage maintained at 15 kV. A focussed beam was used for the minerals while, in order to reduce Na loss during analysis, a defocused beam was used for the glasses. To further reduce Na loss, this element was analysed first. The precision of the Cl and S analyses was established by replicate analyses of glass standards (basaltic and rhyolitic glasses).

The compositions of olivine-hosted glass inclusions in basaltic scoria were obtained with a 8 nA sample current for major elements (acquisition time: 10 s, except for iron: 30 s) and a 30 nA sample current for chlorine and sulphur (acquisition time: 50 s), whereas analyses of olivine-hosted glass inclusions in mantle xenoliths were performed with a 6 nA sample current and different acquisition times: Si, Na, Al, K and Ca for 10 s, Mg for 70 s, Cl for 80 s, and Ti and Fe for 100 s. Both reproducibility and accuracy of the S measurements were tested on the Alv981R23 basaltic glass. Variations in the wavelength of S kα X-ray as a function of the oxidation state of sulfur in silicate glasses were taken into account for S analyse (Métrich and Clocchiatti 1996).

Daughter and host minerals analyses were carried out with a 15 nA sample current and an acquisition time of 10 s, except for Ni in the host olivine, which was analysed for 50 s with a 30 nA current.

Laser ablation-ICP-MS

Trace-element compositions of the largest (> 50 μm in diameter) melt inclusions in scoria were obtained by laser ablation-ICP-MS analyses. These measurements were carried out at the LMV, using an ICPMS VG PQ2+ coupled with a frequency-quadrupled Nd: YAG laser that produces a UV wavelength at 266 nm. For this procedure, the melt inclusions were analysed with a 120-s acquisition time, a laser frequency of 4 Hz and a crater size varying from 40 μm to 80 μm according to the size of the inclusion. Background count rates were first

measured for 30 s before ablation commenced, and this signal was integrated to perform a background correction. Before and after each melt inclusion ablation, two analyses of the reference material NIST 612 were performed in order to test and correct a possible signal variation. BCR (Basalt of Columbia River) USGS glass standards were analysed as unknowns to test accuracy of the analyses. Trace element concentrations were corrected for variations in ablation efficiency between sample and standard by the use of a minor isotope of Ca (^{43}Ca) as an internal standard. CaO concentrations in the melt inclusions were determined previously by electron microprobe (Sect. 3.3). The precision of the Laser Ablation-ICP-MS results are within ±5% for all elements of BCC5(1) and BCC5(2) and within 7% for all elements of BR41 except for Rb (19%) and Y (10%).

Sample description

Basaltic scoria and mantle xenoliths

Scoria samples were found in pyroclastic layers from the terminal strombolian cone of Puy Beaunit. They were naturally quenched during eruption, thus ensuring minimum post-entrapment reactions inside the inclusions. They contain phenocrysts of olivine ($Fo_{80\text{-}86}$) and clinopyroxene ($Wo_{42}En_{47}Fs_{12}$). The olivine phenocrysts sometimes contain chromium spinel inclusions. The groundmass is composed of plagioclase (An_{57}), olivine (Fo_{70}) and magnetite (Table 1).

According to its estimated modal composition, the studied xenolith can be classified as anhydrous spinel lherzolite. It has a protogranular texture (Mercier and Nicolas 1975) and the main phase (Table 1) is olivine, which occurs as porphyroclasts (Fo_{90}, NiO∼0.38 wt%) with undulatory extinction (kink band). Orthopyroxene porphyroclasts (En_{90}) show exsolution lamellae of clinopyroxene. The spinels are chromium-rich (27–35 wt% Cr_2O_3) and occur as rounded interstitial porphyroclasts. The neoblastic texture is poorly developed around the minerals.

Melt inclusions

Melt inclusions in scoria phenocrysts (type I melt inclusions)

Type I melt inclusions are found in both olivine and clinopyroxene phenocrysts, but here we have focussed on the melt inclusions in the most forsteritic olivine (Fo_{85}). They occur mostly as randomly distributed droplets, a feature that is typical of primary inclusions formed during growth of their host phase (Roedder 1984). They vary in size from 20 μm to 70 μm and generally have a regular shape (Fig. 2a), subordinate to the host mineral crystallography, sometimes even producing faceted negative crystal cavities (Fig. 2c). Most of the melt inclusions contain one or sometimes more gas bubbles, which are predominantly composed of CO_2 as verified by cryometric experiments. The ratio ($Volume_{bubble}/Volume_{inclusion}$) is kept roughly constant (except for the few that contain several shrinkage bubbles). Sulphide globules were identified on the edge of several inclusions. Some decrepitation halos and hourglass inclusions (i.e., inclusions that are connected to the outside of the host by a capillary) were also observed.

The inclusions are generally partially crystallised (Fig. 2b) and contain micrometer-size "daughter" minerals (Table 2) crystallized from the trapped melt during slow cooling. The first mineral to crystallise is the host

Table 1 Average mineral compositions of the lherzolite nodule and scoria of Puy Beaunit

	Lherzolite				Scoria					
	Ol	Opx	Cpx	Sp	Ol (P)	Cpx (P)	Ol (M)	Pl (M)	Mt	Sp (In)
SiO_2	40.57	56.02	53.13	0.02	39.25	47.94	37.99	53.55	2.15	0.10
TiO_2	0.01	0.03	0.08	0.04	0.02	1.67	0.04	0.14	19.23	1.84
Al_2O_3	0.01	2.36	2.88	34.81	0.04	7.42	0.03	28.33	3.4	22.06
Cr_2O_3	0.01	0.39	0.88	30.77	0.03	0.22	0.09	0.02	0.19	33.78
Fe_2O_3	–	0.31	1.03	5.12	–	1.99	–	0.73	24.95	11.51
FeO	9.41	6.06	1.42	11.96	14.38	5.79	25.04	0.00	43.60	16.90
MnO	0.14	0.15	0.07	0.17	0.21	0.13	0.44	0.02	0.75	0.20
MgO	48.65	33.73	16.58	16.41	46.03	13.20	36.01	0.09	3.55	12.90
CaO	0.07	0.47	23.39	0.01	0.24	20.49	0.31	11.78	0.48	0.02
Na_2O	0.01	0.01	0.55	0.01	–	0.67	0.02	4.60	0.24	–
K_2O	0.01	0.01	0.01	0.01	–	0.01	0.01	0.51	0.19	–
NiO	0.38	–	–	–	0.15	–	–	–	–	–
Fo	90.1	–	–	–	84.5	–	70.2	–	–	–
An	–	–	–	–	–	–	–	57.2	–	–
Wo	–	0.9	47.2	–	–	41.5	–	–	–	–
En	–	90.0	50.3	–	–	46.9	–	–	–	–
Fs	–	9.1	2.5	–	–	11.6	–	–	–	–

Ol (P) olivine phenocryst, *Ol (M)* olivine microlite, *Cpx (P)* clinopyroxene phenocryst, *Pl (M)* plagioclase microlite, *Opx* orthopyroxene, *Mt* magnetite; *Sp (In)* spinel included in olivine

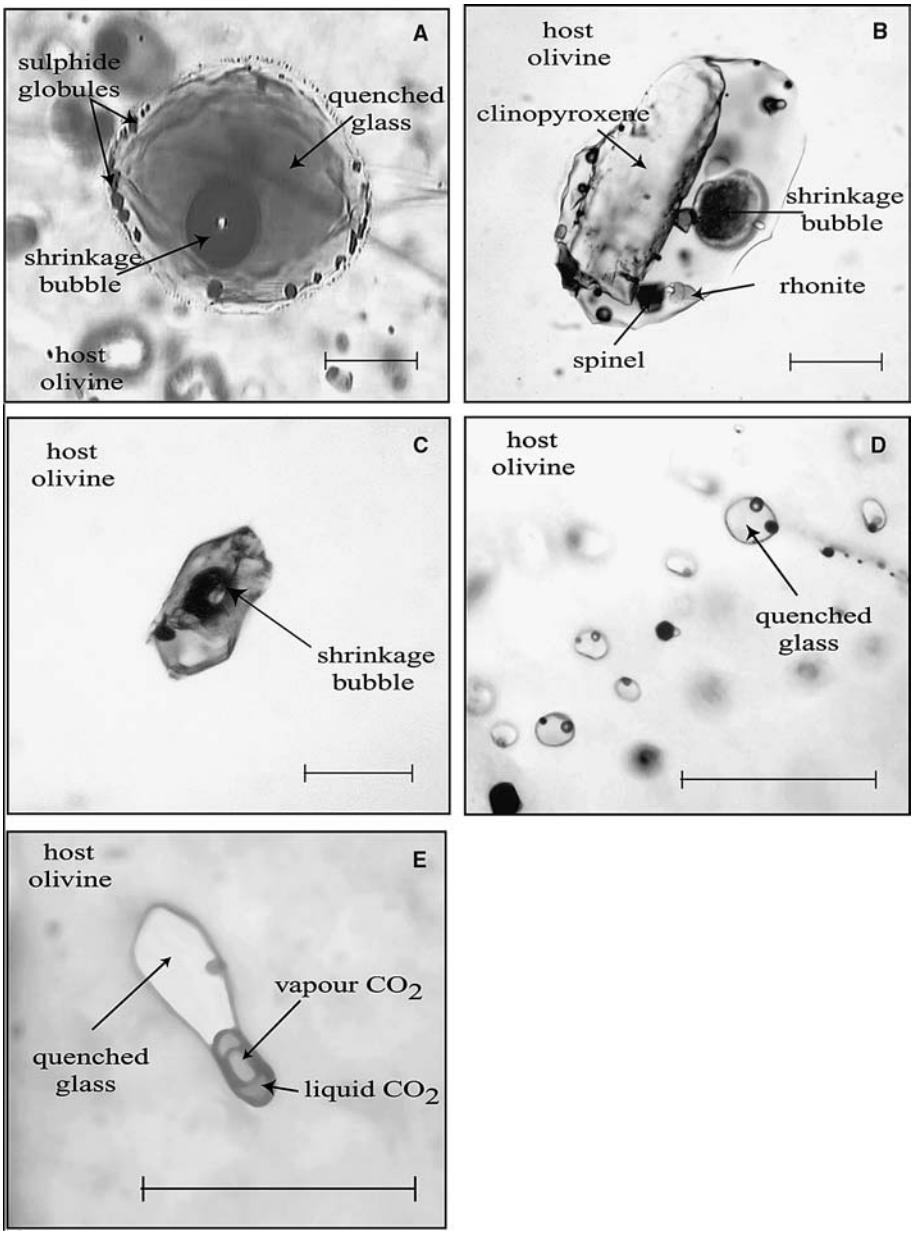

Fig. 2 Transmitted-light photomicrographs of olivine phenocrysts showing the general characteristics of type I and type II melt inclusions. *Bar scale* is 20 μm. **a** Type I melt inclusions containing quenched glass, a shrinkage bubble and sulphides globules outlining the rim of the inclusion. **b** Photomicrograph of type I melt inclusion containing "daughter" minerals formed by closed-system crystallisation during natural cooling. **c** Crystallised type I melt inclusion with negative crystal shape, a secondary feature that results from minimization of the interfacial energies. **d** Typical secondary type II melt inclusions in olivine occurring along healed fracture planes. **e** Multiphase type II melt inclusion containing silicate glass associated with CO_2 fluid inclusion

olivine on the inclusion walls but this mineral does not appear as individual minute crystal inside the inclusion. The second phase to crystallise inside the inclusions is diopside ($Wo_{45–48}$ $Fs_{0–10}$ $En_{40–55}$), which appears as the dominant daughter phase. It occurs as euhedral, prolate-type crystals in the largest inclusions or forms aggregates in the smallest inclusions. The most developed diopside crystals are zoned with increasing Al_2O_3 and TiO_2 and decreasing MgO and CaO from core to rim. It should be noted that the daughter clinopyroxenes have compositions remarkably similar to the clinopyroxene phenocrysts of the more basaltic lavas of the Chaîne des Puys. Daughter plagioclases vary in composition from An_{55} to An_{68} and generally show globular forms.

Rhönite, a relatively uncommon anhydrous mineral typically found as a minor constituent of undersaturated alkaline igneous rocks, was also identified in melt inclusions from electron microprobe analyses. In the Chaîne des Puys lavas, rhönite has been interpreted as a low-pressure amphibole dehydration-destabilisation product (Maury et al. 1980). It is characterized by high concentrations for TiO_2 (~8.5 wt%) and CaO (~12 wt%) but a low concentration for SiO_2 (~25 wt%) and an alkali component of ~ 1 wt%. In Puy Beaunit melt inclusions, rhönite crystals have a globular form and are always associated with other daughter phases, such as clinopyroxene. Their occurrence probably reflects high-degrees of closed-system differentiation inside the inclusions, which could generate a daughter mineral paragenesis different from that of the host basalt. It also suggests an initially very low water content for the melt inclusions (Boivin 1980).

Table 2 Average analyses (wt%) of "daughter" mineral phases inside melt inclusions trapped in olivine phenocrysts from scoria of Puy Beaunit

	Cpx	Pl	Rh
SiO_2	43.91	50.36	25.07
TiO_2	3.48	0.66	8.68
Al_2O_3	9.1	26.95	17.88
Cr_2O_3	0.17	0.02	0.40
Fe_2O_3	4.83	2.51	9.52
FeO	2.8	0.03	11.18
MnO	0.11	0.04	0.14
MgO	12.08	0.84	13.89
CaO	22.16	11.83	12.12
Na_2O	0.54	4.18	0.92
K_2O	0.04	0.89	0.04
An	–	58.2	–
Wo	45.7	–	–
En	48.1	–	–
Fs	6.2	–	–

Cpx clinopyroxene, *Pl* plagioclase, *Rh* rhönite

A high-temperature experimental study was carried out on partially crystallised melt inclusions. Complete homogenisation of melt inclusions (i.e., disappearance of the shrinkage bubble) was not achieved even at high temperature >1,400°C. This persistence of bubbles inside the inclusions during the heating experiments could indicate fluid oversaturation of the inclusions (that is, the presence of primary bubbles trapped along with melt when the inclusions formed) or, more likely, reflect the fact that the melt inclusions do not behave as purely isochoric systems during heating; because of the elastic behaviour of the inclusions, there remains a difference between the initial pressure of trapping and the internal pressure of the inclusions at high T (Schiano and Bourdon 1999) that prevents from complete homogenisation.

Therefore, an alternative method was used, which involved heating the inclusions to the melting point of their last daughter crystals followed by quenching. The melting temperatures vary from 1,225°C to 1,245°C (±10°C) and can be considered as minimum values for the trapping temperature. Note however, that these temperatures are in good agreement with those (between 1,215°C and 1,260°C) obtained using the olivine-melt geothermometer of Ford et al. (1983).

The chemical compositions of type I melt inclusions (Table 3) were determined by analysing unheated glass inclusions that contained no enclosed microphase and heated melt inclusions, after a careful microscopic observation established the absence of microphases that may have formed during the quenching process. For unheated inclusions, post-entrapment reactions occurring inside the inclusions are restricted to slight precipitation of the host phase on the inclusion walls. Correction for this post-entrapment crystallisation was made by incrementally adding olivine in Fe–Mg equilibrium (assuming $K_D^{ol/liq} = (X^{ol}_{Fe*}X^{liq}_{Mg})/(X^{ol}_{Mg}X^{liq}_{Fe*})$ is 0.30 ± 0.03 (Roeder and Emslie 1970) and Fe_{total} as FeO) until the liquidus olivine is identical to the host olivine. The amount of host olivine added to the glass inclusions vary between 7 wt% and 12 wt%.

In primitive olivine phenocrysts (Fo_{85}), the inclusions have alkali-basalt compositions characterised by vari-

Table 3 Representative major element analyses (wt%) of heated and unheated type I melt inclusions trapped in olivine phenocrysts. The Normative compositions are also indicated (the ratio of FeO to Fe_2O_3 is adjusted according to Le Maître 1976)

Sample name	Unheated type I melt inclusions						Heated type I melt inclusions				
	BN5-A2	BCA33	BNol5	BN18-J3	BNol7(1)	BCA11	Plot 10a	Plot 10b	Plot 11	Plot 12a	Plot 12b
SiO_2	45.4	46.29	45.09	44.43	44.23	43.84	43.46	43.68	43.73	43.01	42.27
TiO_2	2.65	2.63	2.81	2.73	2.73	3.33	2.78	2.89	3.09	3.15	3.21
Al_2O_3	14.85	15.86	14.65	15.49	14.62	15.82	15.53	16.00	15.51	16.04	15.63
MnO	0.04	0.06	0.22	0.12	0.15	0.06	0.11	0.11	0.13	0.09	0.15
FeO	9.08	7.32	9.07	7.55	8.69	8.13	8.62	8.61	8.2	8.74	8.82
MgO	9.94	7.62	9.08	8.02	9.21	8.65	8.63	8.84	8.46	8.13	8.09
CaO	11.97	12.31	12.07	12.76	12.5	13.28	13.16	12.96	13.16	13.56	13.52
Na_2O	3.18	3.68	3.31	3.97	3.39	3.57	3.91	3.86	3.45	3.8	3.85
K_2O	1.55	2.12	1.58	1.71	1.56	1.5	1.89	1.75	1.64	1.67	1.62
Cl (ppm)	1,740	1,800	1,870	1,755	1,730	1,470	1,575	1,550	1,420	1,530	1,510
S (ppm)	1,500	1,370	1,340	1,320	1,800	1,420	1,740	1,810	1,625	1,620	1,660
Sum	98.98	98.99	99.23	97.91	98.4	99.31	99.27	99.66	98.62	99.34	98.34
Fo host	84.9	85.1	84.1	85.1	84.8	85.2	85.2	85.2	85.3	85.2	85.2
Normative composition											
Or	9.52	12.5	9.3	10.1	9.2	8.9	0.5	3.7	8.9	0.0	0.0
Ab	7.09	5.3	6.2	1.3	2.7	0.1	0.0	0.0	0.0	0.0	0.0
An	21.61	20.5	20.5	19.4	20.1	22.7	19.2	21.2	22.3	21.8	20.6
Ne	10.92	13.9	11.8	17.5	14.1	16.4	17.9	17.7	15.8	17.4	17.7
Di	31.5	32.2	31.4	34.9	33.4	34.2	36.7	34.4	34.2	36.2	35.1
Ol	9.73	5.5	9.9	5.6	9.2	6.7	6.9	7.9	6.8	5.8	6.3
Mt	3.92	3.1	3.7	3.1	3.5	3.2	3.4	3.4	3.2	3.4	3.4
Ilm	5.44	5.1	5.3	5.2	5.2	6.3	5.3	5.5	5.9	5.9	6.1

Or orthoclase, *Ab* albite, *An* anorthite, *Ne* nepheline, *Di* diopside, *Ol* olivine, *Mt* magnetite, *Ilm* ilmenite

able contents of SiO_2 (42,5–48 wt%), Al_2O_3 (14,5–17 wt%) and CaO (12–13.5 wt%), with the Mg# ($Mg/Mg+Fe^{2+}$) varying from 63% to 66%. All melt inclusions have nepheline and olivine normative compositions. Note that they are relatively rich in chlorine (from 1,500 ppm to 2,000 ppm) and sulphur (1,000 ppm to 2,200 ppm). Unheated glassy melt inclusions and heated melt inclusions have similar compositions, indicating that during the heating experiment no significant interaction between the inclusions and the host minerals has taken place.

Trace element analyses of unheated type I glassy inclusions are reported in Table 4 and illustrated in Fig. 3. The abundance patterns of the melt inclusions are coherent and differ from each other primarily by the enrichment factors of the very and moderately incompatible elements. All the melt inclusions have high concentrations of large-ion lithophile elements (LILE; K, Rb, Ba, Th, U) and light rare-earth elements (LREE). Note also that when elements are arranged by relative compatibility in oceanic basalts (Hofmann 1997) and normalized to primitive-mantle values (Hofmann 1988), no significant anomaly that disturb the otherwise fairly smooth shape of the patterns is observed (Fig. 3). These features are entirely compatible with a generation by partial melting of an enriched mantle source comparable to those generating ocean-island or continental basalts. This is supported by the high Ti/Zr ratios (>60) of the melt inclusions, which are similar to the values obtained for alkali basalts (Sun and Mc Donough 1989).

Melt + fluid inclusions in lherzolite porphyroclasts (type II melt inclusions)

Type II melt inclusions occur as trails outlining secondary fractures cutting through one or more minerals of the spinel peridotite, crosscutting grain boundaries. Their diameter varies in size from 3 μm to 10 μm (Fig. 2d). They generally have rounded shapes with slightly curved walls, but often were deformed and have become vermicular, sigmoid or elongated. Most of the inclusions contain quenched glass and one (or very rarely several) two-phase (gas/liquid) CO_2 bubble(s). A few inclusions also contain micrometer-size daughter minerals.

Abundant secondary CO_2 fluid inclusions also occur in the minerals of the xenolith samples. They are less than 15 μm in size, subspherical or elongated in shape, and contain either coexisting vapour and liquid phases or only a liquid phase. They are located in healed linear fractures often crosscutting each other, indicating that the host crystals have experienced several episodes of shear deformation.

An important observation to be made is that the fluid inclusions are often associated with type II melt inclusions along the same trails. In addition, multiphase inclusions consisting of silicate glass and CO_2-rich fluid (Fig. 2e), and melt inclusions and CO_2 inclusions linked by necks, are also observed. These features imply a cogenetic relationship between melt inclusions and fluid inclusions and suggest that the two types of inclusions have been trapped from an immiscible mixture of silicate melt and CO_2.

The chemical composition of type II melt inclusions (Table 5) was determined by analysing unheated glass inclusions, selected after a careful microscopic study established that they contained no daughter minerals. Normative compositions of type II melt inclusions are characterized by high-olivine and nepheline components. They typically contain high concentrations of SiO_2 (55–59 wt%), Al_2O_3 (20–23 wt%), Na_2O (5–6.5 wt%) and K_2O (2–3.5 wt%), and low concentrations of TiO_2 (<1 wt%), FeO (2–3 wt%) and MgO (2–3.5 wt%). With regards to volatile elements, type II inclusions contain high levels of chlorine (2,000–5,000 ppm), however the sulphur contents never exceed 200 ppm. It should be noted that with the sum of the analyses always close to 100 wt%, the possibility of significant amounts of dissolved water can be excluded.

Table 4 Trace element compositions (ppm) of type I melt inclusions

Sample name	BCC5 (1)	BCC5 (2)	BR41
Rb	–	–	42
Ba	540	561	319
Th	5.6	6.2	3.2
U	1.69	1.82	0.91
Nb	64	79	34
La	50	54	25
Ce	98	106	52
Nd	38	42	22
Sr	510	648	396
Sm	7.1	7.3	4.6
Hf	4.2	4.8	3.0
Zr	184	216	125
Eu	2.12	2.29	1.40
Dy	4.8	5.0	3.9
Y	23.0	23.7	18.7
Er	2.4	2.5	2.0
Yb	2.3	2.3	1.9

Discussion

In order to illustrate the differences between type I and type II melt inclusions, their compositions are plotted in a SiO_2–FeO + MgO–alkalis ternary diagram (Fig. 4). Type II melt inclusions plot within the field of previously published data for olivine-hosted melt inclusions in mantle xenoliths from intraplate (oceanic and continental) settings (Schiano and Clocchiatti 1994; Schiano and Bourdon 1999). By contrast, compositions of type I melt inclusions are significantly less Si-rich and at the same time contain higher total FeO + MgO. Note also that type II melt inclusions have higher Na_2O and K_2O contents, which is the reason for their nepheline-olivine normative compositions despite their silica-rich character. Hence, the two types of melt inclusions are texturally different, occur in phenocrysts of diverse origins, and

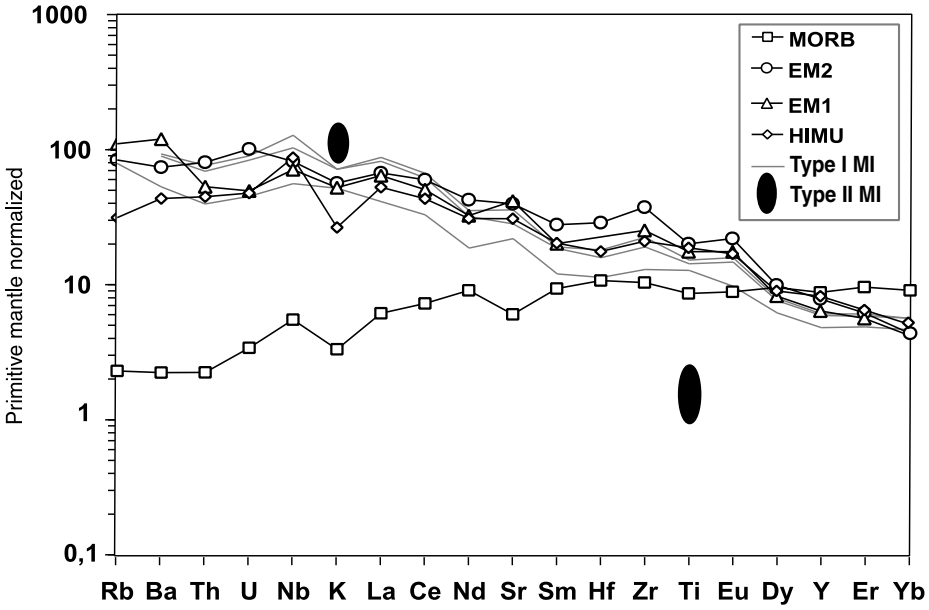

Fig. 3 Primitive mantle-normalised trace element variation diagrams for type I melt inclusions. Compositions are normalized to the primitive mantle composition of Hofmann (1988) and the trace-elements are arranged by relative incompatibility in oceanic basalts (Hofmann 1988; Sun and McDonough 1989; Schiano et al. 1993). Trace element variation diagrams for type I melt inclusions (in *grey*) are compared with typical patterns defined for the average N-MORB of Hofmann (1988), HIMU, EM1- and EM2-type OIB composition (Woodhead 1996; Sun and McDonough 1989; Hémond et al. 1994). Fields of normalized Ti and K values for type II melt inclusions are also shown for comparison

present distinct chemical compositions. We therefore conclude that they relate to distinct petrogenesis processes. Models for the origin of the compositions of olivine-hosted melt inclusions in scoria and mantle nodules from Puy Beaunit are evaluated in the following discussion.

The origin of type I melt inclusions

In Fig. 5, we have compared the major elements compositions of olivine-hosted type I melt inclusions with the whole rocks trend for the Chaîne des Puys volcanoes. Whole rocks vary in composition from moderately potassic alkali basalt to trachyte and can be interpreted relatively simply in terms of fractionation of an olivine-clinopyroxene-spinel assemblage, followed by progressive extraction of oxides, plagioclase and amphibole

Table 5 Representative major-element analyses (wt%) of type II melt inclusions in olivine phenocrysts in ultramafic xenolith from Puy Beaunit

Sample name	10p	10r	8b	8f	8j	3a	6b	6c
SiO_2	59.40	58.11	57.29	57.15	57.64	57.76	58.64	57.83
TiO_2	0.35	0.44	0.47	0.46	0.42	0.47	0.83	0.64
Al_2O_3	20.40	21.03	20.99	21.54	21.87	21.58	20.50	21.54
MnO	0.00	0.00	0.00	0.11	0.09	–	–	–
FeO	2.14	2.02	2.53	2.20	2.31	2.35	2.21	2.30
MgO	2.34	2.27	2.61	2.32	2.49	2.54	2.37	2.43
CaO	5.68	6.27	5.65	6.65	6.58	6.83	5.26	4.54
Na_2O	6.36	5.73	6.55	6.32	6.38	5.75	5.67	6.24
K_2O	3.34	3.13	2.97	2.74	2.31	2.63	3.71	3.52
Cl (ppm)	4,730	4,790	4,320	4,250	4,230	3,950	2,960	2,910
S (ppm)	220	160	140	380	280	–	–	–
Sum	100.51	99.49	99.63	99.94	100.54	100.29	99.47	99.33
Fo host	90.0	90.0	90.0	90.0	90.0	90.0	90.0	90.0
Normative compositions								
Or	19.8	18.5	17.6	16.2	13.7	15.5	21.9	20.8
Ab	47.5	44.9	43.7	52.5	46.1	45.1	45.6	44.9
An	19.1	24.3	20.8	24.1	25.9	26.9	20.7	21.5
Ne	1.5	0.0	4.6	4.2	2.6	0.3	0.1	3.1
Di	6.4	4.7	5.4	6.9	5.4	5.7	4.4	0.8
Ol	4.4	3.2	5.6	4.3	5.3	5.2	4.7	6.4

Normative compositions are indicated: *Or* orthoclase, *Ab* albite, *An* anorthite, *Ne* nepheline, *Di* diopside, *Ol* olivine

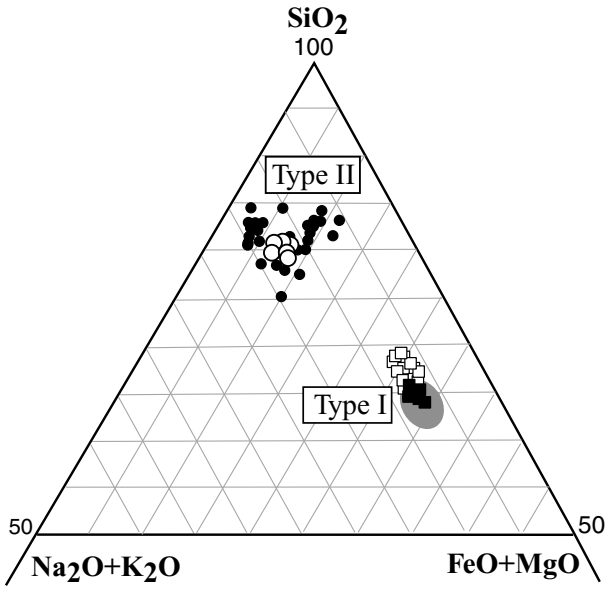

Fig. 4 Composition of heated (*black square*) and unheated (*open square*) type I melt inclusions compared with type II melt inclusions (*open circle*). Also indicated for comparison with type II melt inclusions are unheated glassy and experimentally rehomogenized melt inclusions trapped in mantle xenoliths from intraplate (ocean and continental) settings (Schiano and Clocchiatti 1994; Schiano and Bourdon 1999) (*black circles*). The compositional field (*grey*) for the type I melt inclusions corrected for post-entrapment Fe-loss (see Fig. 5 caption), is also reported

(Foury 1983). In binary diagrams, the type I melt inclusions fall on the primitive end of the arrays of whole rock compositions; they are thus likely to represent preserved aliquots of primitive, parental melts from which the suite of magmas from the Chaîne des Puys have evolved. Note, however, that they cannot be identified as "primary" mantle magmas (i.e. unmodified partial melts of peridotite source regions) because forsterite values (Fo_{85}) of the host olivine phenocrysts suggest not that they are in equilibrium with mantle peridotite.

It should also be noted that the melt inclusions are depleted in FeO compared with the whole-rock trend of the Chaîne des Puys (Table 3). The depletion affects both heated and unheated glassy melt inclusions, indicating that this feature cannot result from the heating procedure. Based on a study of experimentally heated melt inclusions, Danyushevsky et al. (2000) have described a potential reequilibration process that can affect the composition of melt inclusions trapped in olivine crystals. According to these authors, diffusive exchange occurs between the residual melt within the inclusion and the host olivine and results in lower FeO and higher MgO contents in the inclusions. As shown in Fig. 5, the Fe-correction only requires minor modifications to the other major elements. This observation and the fact that the most primitive olivine phenocrysts observed in the Chaîne des Puys are also in the $Fo_{86–85}$ range (Maury et al. 1980) supports our hypothesis that

Fig. 5 Major element variation diagrams for heated (*black square*) and unheated (*open square*) type I melt inclusions compared with the trend defined by the lavas of the Chaîne des Puys (*grey squares*) (P. Boivin compilation). Also shown in the diagram are the host products of Puy Beaunit (*black circle*) and type I melt inclusions (*open diamond*) corrected for post-entrapment Fe-loss according to the procedures outlined by Danyushevsky et al. (2000); i.e., assuming 10, 67 wt% FeO (a value representative of the host lavas) in the melt inclusions

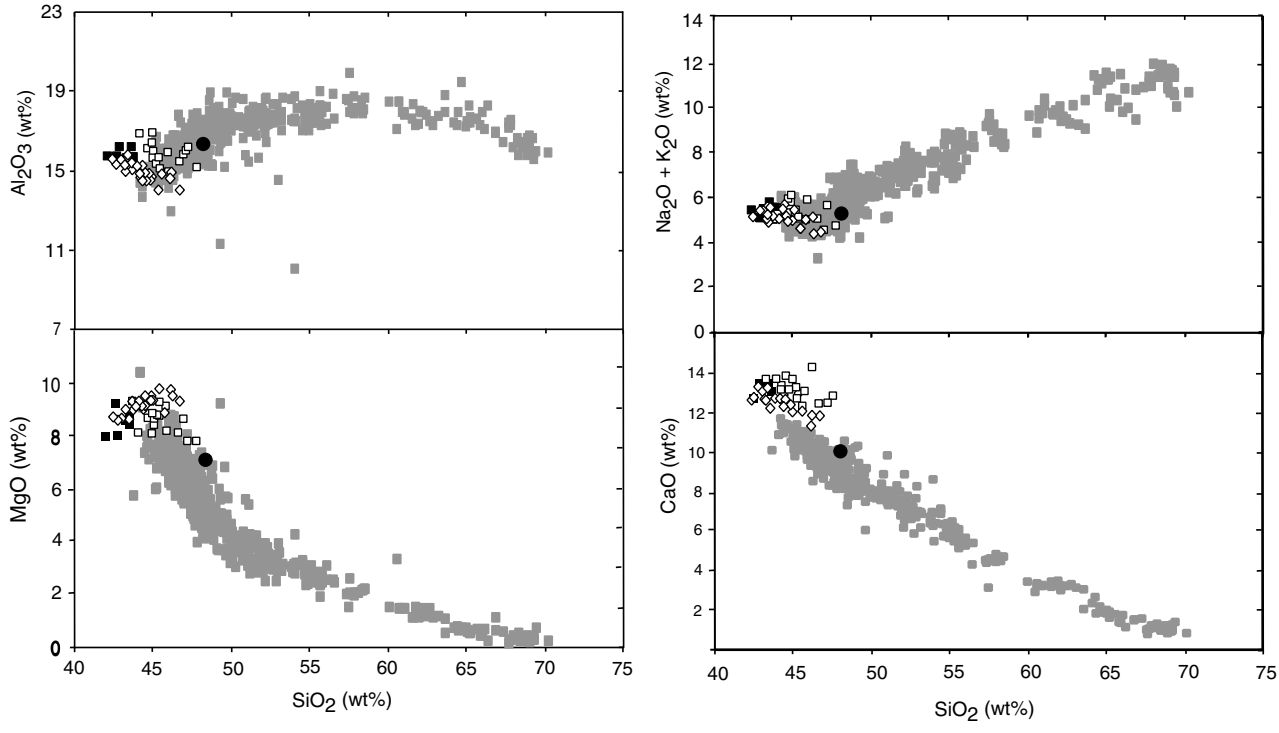

type I melt inclusions represent early liquids that could provide reliable information on the composition and formation conditions of Puy Beaunit primitive mantle derived magmas and the conditions at which they have formed.

Figure 3 illustrates the primitive-mantle normalised trace-element patterns for the melt inclusions compared with the estimated average N-MORB composition of Hofmann (1988) and the representative HIMU, EM1- and EM2-type OIB compositions from Mangaia Island (Woodhead 1996), Gough Island (Sun and McDonough 1989) and Society Island (Hémond et al. 1994), respectively. The trace elements are ordered following the incompatibility sequence determined for oceanic basalt melting (Hofmann 1988; Sun and McDonough 1989; Schiano et al. 1993). All the inclusions have fundamentally different trace-element patterns from N-MORB, indicating that they do not sample predominantly depleted upper mantle regions similar to those sampled by basalts along mid-ocean ridges. They require the existence of a mantle source enriched in incompatible elements relative to normal MORB. They also do not show negative anomalies for high-field strength elements (HFSE) considered as evidence for a subduction-related origin. Their trace element features are remarkably similar to all OIB with a EM2 or EM1-type isotopic signature (i.e., very high Sr isotope ratios); that is, they display high normalized concentrations of incompatible elements and they lack the relative depletions in K, Rb and Cs that characterize HIMU-type (the other isotopically extreme signature) basalts (Weaver 1991; Allègre et al. 1995; Hofmann 1997). The involvement of an EM2-type mantle component in the source of the type I melt inclusions is also supported by plots of ratios involving highly incompatible elements (with bulk solid/melt partition coefficients $\ll$ melt fraction) (Fig. 6). It is generally accepted that the trace-element characteristics of EM2-type magmas reflect derivation from a source that may incorporate small amounts of sediments (1–2%) (see Hofmann 1997, and references therein).

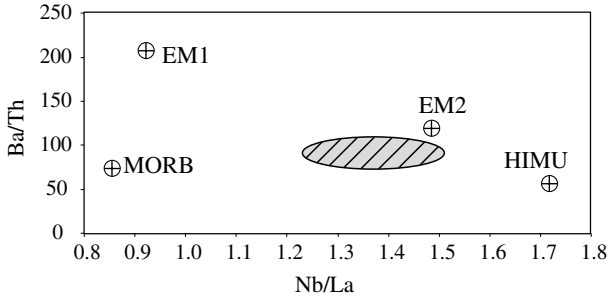

Fig. 6 Ba/Th versus Nb/La diagram comparing type I melt inclusions (*grey dashed field*) with estimated compositions of the source of N-type MORB, HIMU-ype and EM-type ocean island basalts (Allègre et al. 1995)

The origin of type II melt inclusions

Previous studies of glass inclusions in peridotite nodules have shown that enclosed melts with compositions similar to the type II melt inclusions, i.e. melts characterized by high concentrations of silica and alkali- oxides along with low concentrations of FeO and MgO (Fig. 4), are a common feature of spinel-lherzolite olivines and orthopyroxenes (e.g., Schiano et al. 1992, 1994; Schiano and Clocchiatti 1994; Schiano and Bourdon 1999). They also established that their compositions do not reflect a hypothetical post-entrapment evolution such as crystallization of reaction minerals between glass and host (e.g., Schiano et al. 1992, 1994). Two main hypotheses have been put forward to explain the origin of these melts. Their compositions, which differ drastically from those of erupted, mantle-derived magmas, have led several authors to propose that they represent end-products of disequilibrium melting processes, such as local incongruent melting of accessory minerals or reactions between infiltrated mafic melts and the surrounding peridotite (e.g. Frey and Green 1974; Zinngrebe and Foley 1995; Yaxley et al. 1997; Neumann and Wulff-Pedersen 1997; Shaw 1999). However, others have suggested that the silica-rich inclusions in mantle minerals are in equilibrium with the surrounding mantle and should represent near-solidus partial melts of peridotite at moderate pressures (e.g., Schiano et al. 1998; Hirschmann et al. 1998; Schiano and Bourdon 1999). The most important issue to address with regard to the origin of these SiO_2-rich melts is therefore the question of equilibrium as disequilibrium melt compositions would have been modified during crystal-melt reactions. Thus are these melts in equilibrium with Mg-rich mantle phase or not?

Direct support for the attainment of equilibrium between silica-rich melt inclusions and their host olivine crystals is given by the multiple saturation experiments of Draper and Green (1997, 1999), which demonstrate that silica-rich liquids with compositions comparable to the type II melt inclusions can be in equilibrium with lherzolite and harzburgite assemblages at upper mantle conditions. Moreover, Falloon et al. (1997) have demonstrated that silicic melts in equilibrium with a peridotitic assemblage (Mg# of olivine ~90) would have nepheline–olivine normative compositions, which is also in agreement with the compositions of type II melt inclusions. Finally, an additional constraint on the composition of silica-rich melts in equilibrium with peridotite residual mineralogy was given by Baker et al. (1996). These authors have shown that increasing total alkali oxide content of silicic melts would decrease the Fe–Mg exchange coefficient ($K_D^{ol/liq} = (X^{ol}_{Fe*}X^{liq}_{Mg})/(X^{ol}_{Mg}X^{liq}_{Fe*})$) to values much lower than the 1 atm value of 0.30 ± 0.03 determined by Roeder and Emslie (1970). As shown in Fig. 7, the $K_D^{ol/Liq}$ calculated for the type II melt inclusions fall on an extension of the trend defined by Baker et al. (1996), supporting thus the hypothesis

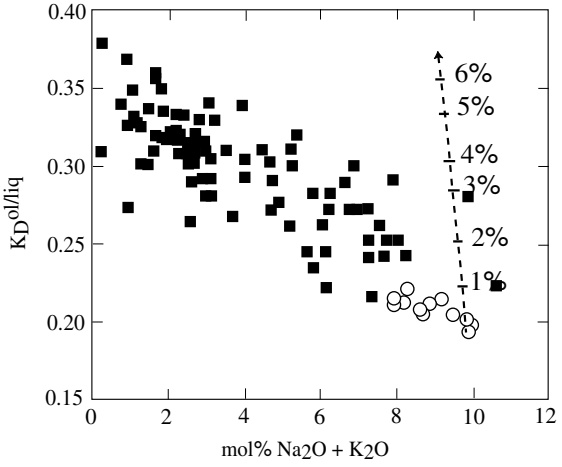

Fig. 7 Plot of olivine-liquid Fe*–Mg K_D values versus total alkali contents (in mol%) comparing type II melt inclusions (*open circles*) with experimental melts of natural and model peridotites (*black squares*) (see Baker et al. 1996 and references therein) (Fe* = total Fe). Also shown for comparison is a trend (*dotted line*, labelled with the extent of crystallization) calculated for progressive post-entrapment crystallisation of the host olivine. With increasing crystallization, the trend clearly extends away from the equilibrium array

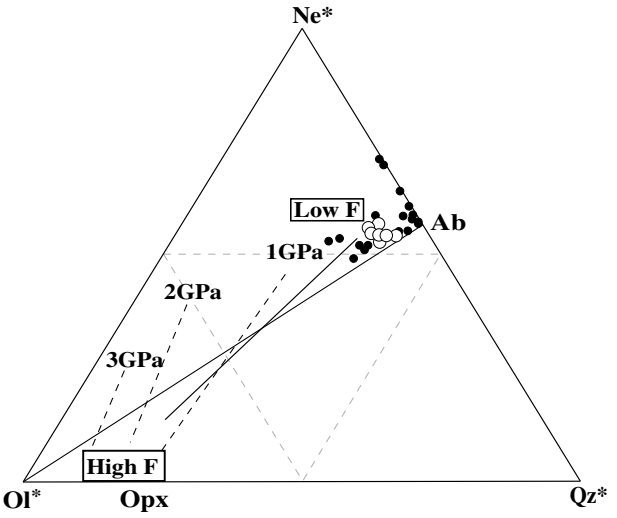

Fig. 8 normative composition of type II melt inclusions (*open circles*) and melt inclusions in olivine porphyroclasts in ultramafic nodules from intraplate settings (*black circles*) plotted in the ternary olivine-nepheline–quartz projection of the basalt tetrahedron. Ne* = Ne + 0.6 Ab, Qz* = Qz + 0.4 Ab + 0.25 Hy, Ol* = Ol + 0.75 Hy. Trends for isobaric melting experiments of spinel-lherzolite are shown for comparison; *dashed-lines* are based on experimental data of Hirose and Kushiro (1993) at 1, 2 and 3 GPa (the degree of melting (F) varying between 5% and 40%) and the solid line corresponds to experimental data of Baker et al. (1995), with revised analyses from Hirschmann et al. (1998) at 1 GPa (*F* varying between 2% and 20%)

that the inclusions contain liquids in equilibrium with their host mantle olivine at upper mantle temperatures and pressures. Both lines of evidence clearly indicate that a disequilibrium process, which can for instance result from decompression melting of the xenolith during ascent, is not a plausible explanation for the origin of the SiO_2-rich melt inclusions identified here.

Type II melt inclusions could represent trapped aliquots of near-solidus partial melts of peridotites, preserved from chemical modification during ascent of their host xenolith (Schiano et al. 1998; Schiano and Bourdon 1999). Following this hypothesis, the silica-rich character of these low melt fractions mainly reflects the reduction in the silica activity coefficient by alkalis at pressures around 1.0 GPa (Hirschmann et al. 1998; Schiano et al. 1998). Indeed, for mantle melts coexisting with an olivine-orthopyroxene-bearing mineral assemblage buffering SiO_2 activity, this decrease is compensated by an increase in the SiO_2 content of the melt. Figure 8 is the olivine-nepheline-quartz ternary projection of the basalt tetrahedron (after the projection scheme described by Irvine and Baragar 1971) on which we have plotted type II melt inclusion compositions along with experimental isobaric trends for dry peridotite (Hirose and Kushiro 1993; Baker et al. 1995). The melt inclusions plot at the end of the trend defined by Baker et al. (1995) for low degree-melts of spinel-lherzolite at 1 GPa, thus supporting our hypothesis that they represent aliquots of low melt fractions of peridotite.

An important additional question regarding the nature of the silica-rich melts observed within mantle minerals from intraplate regions relates to their ability of causing chemical and/or mineralogical changes in the upper mantle composition. On the basis of their high concentrations in incompatible elements, various authors have suggested that these melts have a high potential as transport agents capable of causing cryptic metasomatism ((i.e., replenishment in lithophile trace-elements) in mantle peridotites (e.g., Draper and Green 1999, and references therein). The evidence presented above that type II melt inclusions are in equilibrium and thus can coexist with peridotite lithologies suggests that these melts could circulate over long distances through the mantle and act as effective agents of large-scale metasomatism. However, Maumus et al. (2004) have recently established from dihedral angle measurements and infiltration experiments that although these SiO_2 and alkali-rich melts could be interconnected in the peridotite matrix, their high viscosity and the low permeability of their matrix will inhibit the melt from segregating and migrating on any significant scale; i.e., a greater scale than their host phases. Therefore, they cannot represent the end-products of large-scale metasomatic processes, but are more likely to be transitional phenomena related to peridotite melting. In addition, the limited ability of these near-solidus melts to segregate strongly suggests that the host xenolith represents the residue of the melting process, which would be in agreement with the interpretation of the silica-rich melt inclusions in spinel-lherzolite nodules from the Comores by Schiano et al. (1998).

An important motivation for this study was to test the hypothesis that olivine-hosted melt inclusions in erupted scoria and mantle nodules have the same origin and could be genetically related. However, the observed differences in major-element chemistry between the two types of melt cannot be simply accounted for by progressive differentiation or melting processes. In addition, we argue that type II melt inclusions are likely to be generated at moderate pressure during incipient melting of their host spinel lherzolite. By contrast, partial melting experiments performed on natural lherzolite (e.g., Hirose and Kushiro 1993) indicate that in order to obtain silica contents as low as those of type I melt inclusions (<44 wt% for the heated inclusions), partial melting should occur at high pressures (≥30 kbar), i.e., in the garnet lherzolite stability field. This implies that the two types of melt relate to distinct melting events that occurred at different depths in the mantle beneath the volcano. If, as discussed above, the trapped melts in olivine phenocrysts from scoria are likely to represent samples of the parental melts from which the evolved magma compositions found at Puy Beaunit are derived, no clear relationship can be drawn between the melts trapped in mantle olivine from the xenolith and the erupted basalts. In addition, the conclusions drawn from the study of type II melt inclusions are valid at the length scale of the host xenolith and may or may not apply at the scale of mantle melting, representing some tens of kilometres.

Conclusion

This study confirms that chemically distinct melts can be preserved in Mg-rich olivine crystals in basalts and associated upper mantle nodules extruded from a single volcano. Melt inclusions trapped in olivine phenocrysts from scoria of Puy Beaunit, a volcano from the Chaîne des Puys volcanic province of the Massif Central, contain primitive alkali-basalt liquids, which are consistent with the compositions expected for parental melts of the Chaîne des Puys magmatic series. Their trace-element signature is indicative of a source that contains small amounts of recycled, continental-derived sediments. In contrast, silicic melts with compositions that differ dramatically from the erupted basalts are preserved as olivine-hosted glass inclusions in peridotite nodules transported to the surface by the Puy Beaunit lavas. They represent near-solidus melts of spinel lherzolite and their compositions reflect the effect of alkali oxides on the silica activity coefficient of the melts. Moreover, their high viscosity which causes their limited segregation ability is an important factor that can explain the absence of a genetic link with the erupted magmas.

Acknowledgments We thank Didier Laporte for supplying the nodule samples, and Jean-Luc Devidal and Michelle Veschambre for technical help. We also acknowledge F. Faure and R. Clocchiatti for helpful discussion. The LA-ICPMS analyses were carried out with the assistance of Gilles Chazot whose help is gratefully acknowledged. Journal reviews by P.J. Wallace and R.L. Nielsen are appreciated. Financial support was provided by the European Community's Human Potential Programme under contract HPNR-CT-2002-0211 (Euromelt). S. Jannot is also grateful for the Conseil Régional d'Auvergne for funding her Ph.D. thesis.

References

Allègre CJ, Schiano P, Lewin E (1995) Differences between oceanic basalts by multitrace element ratio topology. Earth Planet Sci Lett 129:1–12

Baker MB, Hirschmann MM, Ghiorso MS, Stolper EM (1995) Compositions of near-solidus peridotite melts from experiments and thermodynamic calculations. Nature 375:308–311

Baker MB, Hirschmann MM, Wasylenki LE, Stolper EM (1996) Quest for low-degree mantle melts. Nature 381:286

Barruol G, Granet M (2002) A tertiary asthenospheric flow beneath the southern French Massif Central indicated by upper mantle seismic anisotropy and related to the west Mediterranean extension. Earth Planet Sci Lett 202: 31–47

Boivin P (1980) Données experimentales préliminaires sur la stabilité de la rhönite à 1 atmosphère. Application aux gisements naturels. Bull Min 103:491–502

Boivin P, Besson JC, BriotT D, Camus G, Goër de Herve A de, Gourgaud A, Labazuy P, Larouzière FD de, Livet M, Mergoil J, Mialler D, Morel JM, Vernet G, Vincent PM (2004) Volcanologie de la Chaîne des Puys Massif Central Français, 4ème édition. le Parc Naturel Régional des Volcans d'Auvergne, 180 p

Danyushevsky LV, Della-Pasqua FN, Sokolov S (2000) Re-equilibration of melt inclusions trapped by magnesian olivine phenocrysts from subduction-related magmas: petrological implications. Contrib Mineral Petrol 138:68–83

Downes H, Dupuy C (1987) Textural, isotopic and REE variations in spinel peridotite xenoliths, Massif Central, France. Earth Planet Sci Lett 82:121–135

Draper DS, Green TH (1997) P-T phase relations of silicic, alkaline, aluminous mantle-xenolith glasses under anhydrous and C–O–H fluid-saturated conditions. J Petrol 38:1187–1224

Draper DS, Green TH (1999) P-T phase relations of silicic, alkaline, aluminous liquids: new results and applications to mantle melting and metasomatism. Earth Planet Sci Lett 170:255–268

Falloon TJ, Green DH, O'Neill HStC, Hibberson WO (1997) Experimental tests of low degree peridotite partial melt compositions: implications for the nature of anhydrous near-solidus peridotite melts at 1 Gpa. Earth Planet Sci Lett 152:149–162

Faure F, Trolliard G, Montel JM, Nicollet C (2001) Nano-petrographic investigation of a mafic xenolith (maar de Beaunit, Massif Central, France). Eur J Mineral 13:27–40

Féménias O, Mercier JC, Demaiffe D (2001) Pétrologie des xénoliths ultramafiques du puy Beaunit (Massif Central français): un gisement atypique du manteau sous-continental?. C R Acad Sci Paris IIA 332:535–542

Féménias O, Coussaert N, Bingen B, Whitehouse M, C.Mercier J-C, Demaiffe D (2003) A Permian underplating event in late- to post-orogenic tectonic setting. Evidence from the mafic-ultramafic xenoliths from Beaunit (French Massif Central). Chem Geol 199: 293–315

Ford CE, Russel DG, Craven JA, Fisk MR (1983) Olivine-Liquid equilibria: temperature, pressure and composition dependance of the crystal/liquid cation partition coefficients for Mg, Fe2+, Ca and Mn. J Petrol 24:256–265

Foury P (1983) Etudes pétrologiques et expérimentales (à une atmosphère) d'une série alcaline continentale de la Chaîne des Puys (M.C.F.). Thesis Univ. B. Pascal, Clermont-Ferrand II, 150 p

Franke W (1989) Variscan plate tectonics in Central Europe-current ideas and open questions. Tectonophysics 169:221–228

Frey FA, Green DH (1974) The mineralogy, geochemistry and origin of lherzolite inclusions in Victorian basanites. Geochim Cosmochim Acta 30:1023–1059
Froidevaux C, Brousse R, Bellon H (1974) Hot Spot in France? Nature 248:749–751
Granet M, Wilson M, Achauer U (1995). Imagine a mantle plume beneath the French Massif Central. Earth Planet Sci Lett 136:281–296
Hémond C, Devey CW, Chauvel C (1994) Source composition and melting processes in the Society and Austral plumes (South Pacific Ocean): Element and isotope (Sr, Nd, Pb, Th) geochemistry. Chem Geol 115:7–45
Hirose K, Kushiro I (1993) Partial melting of dry peridotites at high pressure: determination of compositions of melts segregated from peridotites using aggregates of diamonds. Earth Planet Sci Lett 114:477–489
Hirschmann MM, Baker MB, Stolper EM (1998) The effect of alkalis on silica content of mantle derived melts. Geochim Cosmochim Acta 62:883–902
Hofmann AW (1988) Chemical differentiation of the Earth: the relationship between mantle, continental crust and oceanic crust. Earth Planet Sci Lett 90:297–314
Hofmann AW (1997) Mantle geochemistry: the message from oceanic volcanism. Nature 385:219–229
Irvine TN, Baragar WR (1971) A guide to the chemical classification of the common volcanic rocks. Can J Earth Sci 8:523–548
Kushiro I, Walter MJ (1998) Mg-Fe partitioning between olivine and mafic-ultramafic melts. Geophys Res Lett 25:2337–2340
Le Maître RW (1976) Some problems of the projection of chemical data into mineralogical classifications. Contrib Mineral Petrol 56:181–189
Lenoir X, Garrido CJ, Bodinier JL, Dautria JM (2000) Contrasting lithospheric mantle domains beneath the Massif Central (France) revealed by geochemistry of peridotite xenoliths. Earth Planet Sci Lett 181:359–375
Matte P (1986) Tectonics and plate tectonics model for the Variscan belt of Europe. Tectonophysics 126:329–374
Maumus J, Laporte D, Schiano P (2004) Dihedral angle measurements and infiltration property of SiO_2-rich melts in mantle peridotite assemblage. Contrib Mineral Petrol 148:1–12
Maury RC, Brousse R, Villemant B, Joron JL, Jaffrezic H, Treuil M (1980) Cristallisation fractionnée d'un magma basaltique alcalin: la série de la Chaîne des Puys (Massif Central, France), I. Pétrologie. Bull Minéral 103:250–266
Mercier JC, Nicolas A (1975) Textures and Fabrics of upper-mantle peridotites as illustrated by xenoliths from basalts. J Petrol 16:454–487
Merle O, Michon L (2001) The formation of the West European Rift: a new model as exemplified by the Massif Central area. Bull Soc Géol France 172:213–221
Métrich N, Clocchiatti R (1996) Sulphur abundance and its speciation in oxidized alkaline melts. Geochim Cosmochim Acta 60:4151–4160
Neumann ER, Wulff-Pedersen E (1997) The origin of highly silicic glass in mantle xenoliths from the Canary Islands. J Petrol 38:1513–1539
Roedder E (1984) Fluid Inclusions. Rev Mineral 2:620
Roeder PL, Emslie RF (1970). Olivine-liquid equilibrium. Contrib Mineral Petrol 29:275–289
Schiano P (2003) Primitive mantle magmas recorded as silicate melt inclusions in igneous minerals. Earth Sci Rev 63:121–144
Schiano P, Bourdon B (1999) On the preservation of mantle information in ultramafic nodules; glass inclusions within minerals versus interstitial glasses. Earth Planet Sci Lett 169:173–188
Schiano P, Clocchiatti R (1994) Worldwide occurrence of silica-rich melts in sub-continental and sub-oceanic mantle minerals. Nature 368:621–624
Schiano P, Clocchiatti R, Joron JL (1992) Melt and fluid inclusions in basalts and xenoliths from Tahaa island, Society archipelago: evidence for a metasomatised upper mantle. Earth Planet Sci Lett 111:69–82
Schiano P, Allègre CJ, Dupré B, Lewin E, Joron JL (1993) Variability of trace elements in basaltic suites. Earth Planet Sci Lett 119: 37–51
Schiano P, Clocchiatti R, Shimizu N, Weis D, Matielli N (1994) Cogenetic silica-rich and carbonate-rich melts trapped in mantle minerals in Kerguelen ultramafic xenoliths : implications for metasomatism in the oceanic upper mantle. Earth Planet Sci Lett 123:167–178
Schiano P, Clocchiatti R, Shimizu N, Maury RC, Jochum KP, Hofmann AW (1995) Hydrous, silica-rich melts in the sub-arc mantle and their relationship with erupted arc lavas. Nature 377:595–600
Schiano P, Bourdon B, Clocchiatti R, Massare D, Varela ME, Bottinga Y (1998) Low-degree partial melting trends recorded in upper mantle minerals. Earth Planet Sci Lett 160:537–550
Shaw CSJ (1999) Dissolution of orthopyroxene in basanitic magma between 0.4 and 2 Gpa; further implications for the origin of Si-rich alkaline glass inclusion in mantle xenoliths. Contrib Mineral Petrol 135:114–132
Sobolev AV, Barsukov VL, Nevsorov VN, Slutsky AB (1980) The formation conditions of the high-magnesian olivines from the monominerallic fraction of Luna 24 regolith. In: Proceedings of the 11th lunar planet science conference, pp 105–116
Sun Ss, McDonough WF (1989) Chemical and isotopic systematics of oceanic basalts: implications for mantle composition and processes. In: Saunders AD, Norry MJ (eds) Magmatism in the Ocean Basins. Geological Society Special Publication, 42:313–345
Villemant B, Joron JL, Jaffrezic H, Treuil M, Maury R, Brousse R (1980) Cristallisation fractionnée d'un magma basaltique alcalin: la série de la Chaîne des Puys (Massif Central, France), II. Géochim Bull Minéral 103:267–286
Weaver BL (1991) Trace element evidence for the origin of ocean-island basalts. Geology 19:123–126
Wilson M, Downes H (1992) Mafic alkaline magmatism associated with the European Cenozoic rift system. Tectonophysics 208:173–182
Woodhead JD (1996) Extreme HIMU in an oceanic setting: the geochemistry of Mangaia Island (Polynesia), and temporal evolution of the Cook-Austral hotspot. J Volcanol Geotherm Res 72:1–19
Yaxley GM, Kamenetsky V, Green DH, Falloon TJ (1997) Glasses in mantle xenoliths from western Victoria, Australia, and their relevance to mantle processes. Earth Planet Sci Lett 148:433–446
Ziegler PA (1982) Geological Atlas of Western and Central Europe. Elsevier, Amsterdam, p 130
Zinngrebe E, Foley SF (1995) Metasomatism in mantle xenoliths from Gees, West Eiffel, Germany: evidence for the genesis of calc-alkaline glasses and metasomatic Ca-enrichment. Contrib Mineral Petrol 122:79–96